# Research Report

# Voltage-gated potassium channels involved in regulation of physiological function in MrgprA3-specific itch neurons

Q2

Min Tang[a,b], Guanyi Wu[a,c], Zhongli Wang[a], Niuniu Yang[a], Hao Shi[a], Qian He[b], Chan Zhu[a], Yan Yang[a], Guang Yu[a], Changming Wang[a], Xiaolin Yuan[a], Qin Liu[d], Yun Guan[e], Xinzhong Dong[f], Zongxiang Tang[a,*]

Q1

[a]College of Basic Medicine, Nanjing University of Chinese Medicine, Nanjing, China
[b]College of Biology and Environmental Sciences, Jishou University, Jishou, China
[c]College of Basic Medicine, Guangxi University of Chinese Medicine, Nanning, China
[d]Department of Anesthesiology, Washington University in St. Louis, USA
[e]Department of Anesthesiology and Critical Care Medicine, Johns Hopkins University Schools of Medicine, Baltimore, MD, USA
[f]Howard Hughes Medical Institute, Johns Hopkins University School of Medicine, Baltimore, MD, USA

ARTICLE INFO

ABSTRACT

Itch is described as an unpleasant or irritating skin sensation that elicits the desire or reflex to scratch. MrgprA3, one of members of the Mrgprs family, is specifically expressed in a subpopulation of dorsal root ganglion (DRG) in the peripheral nervous system (PNS). These MrgprA3-expressing DRG neurons have been identified as itch-specific neurons. They can be activated by the compound, chloroquine, which is used as a drug to treat malaria. In the present study, we labeled these itch-specific neurons using the method of molecular genetic markers, and then studied their electrophysiological properties. We also recorded the cutaneous MrgprA3$^-$ neurons retrogradely labeled by DiI dye (MrgprA3$^-$-DiI). We first found that MrgprA3$^+$ neurons have a lower excitability than MrgprA3$^-$ neurons (MrgprA3$^-$-non-DiI and MrgprA3$^-$-DiI). The number of action potential (AP) was reduced more obviously in MrgprA3$^+$ neurons than that of in MrgprA3$^-$ neurons. In most cases, MrgprA3$^+$ neurons only generated single AP; however, in MrgprA3$^-$ neurons, the same stimulation could induce multiple AP firing due to the greater voltage-gated potassium (Kv) current existence in MrgprA3$^+$ than in MrgprA3$^-$ neurons. Thus, Kv current plays an important role in the regulation of excitability in itch-specific neurons.

© 2016 Published by Elsevier B.V.

Q3

## 1. Introduction

Itch (or pruritus) is an unpleasant or irritating skin sensation that elicits the desire or reflex to scratch (Ikoma et al., 2006). The itch signal is generated at the periphery primary sensory neurons (DRG or trigeminal ganglia) and then sent to the spinal cord via their central axons (Paus et al., 2006). Itch and pain sensations are mainly mediated by small-diameter DRG neurons with unmyelinated C fibers (Basbaum et al., 2009; Ikoma et al., 2006). A broad overlap is shared between pain- and itch-related peripheral mediators or receptors; and some similar mechanisms of neuronal sensitization also happen in the peripheral nervous system (PNS) and central nervous system (CNS) (Ikoma et al., 2006; Schmelz, 2005). Itch and pain, however, are two distinct sensations; each can elicit different behavioral responses such as scratching and withdrawal respectively (Klein et al., 2011; Liu and Ji, 2013).

Mrgprs genes (aka Mrg/SNSR) are specifically expressed in subsets of small-diameter neurons in DRG and trigeminal ganglia. They encode a large family of G protein-coupled receptors (GPCRs) consisting of more than 50 members of the mouse genome (Dong et al., 2001; Zylka et al., 2003). Recent studies have indicated that Mrgprs function as receptors for certain chemical pruritogens and mediate itch-associated behavior. For example, β-alanine elicits histamine-independent itch through activation of MrgprD receptor-expressing neurons (Liu et al., 2012). BAM8-22, an endogenous bovine adrenal medulla peptide, evokes itch through direct activation of MrgprC11 receptors in DRG (Sikand et al., 2011). MrgprA3 is a member of the Mrgprs genes family. Our previous study indicated that MrgprA3 is a chloroquine (CQ)-specific receptor, which directly mediates the activation of MrgprA3$^+$ neurons and induces itching behavior in mice (Liu et al., 2009). MrgprA3$^+$ neurons can be activated by multiple chemical pruritogens—CQ, histamine, SLIGRL, BAM8-22, ET-1 and α-Me-5HT—to induce itch. Ablation of MrgprA3$^+$ neurons is able to reduce mouse itch but not pain behavior. When Transient Receptor Potential Vanilloid type 1 (TPRV1), a non-selective cation channel, was specifically expressed in MrgprA3$^+$ neurons, the activation of MrgprA3$^+$ neurons with capsaicin evoked itch but not pain behavior. Specifically, the peripheral fibers of MrgprA3$^+$ neurons exclusively innervate the epidermis of skin but are absent from the rest of body, strongly supporting that itch sensation arises from skin but not deep tissue. Thus, MrgprA3$^+$ neurons are defined as a subpopulation of itch-specific neurons (Han et al., 2013).

Itch sensation, which is evoked by pruritic chemical agents, begins with electrical activity in a subset of peripheral cutaneous nociceptors or pruriceptors and a subpopulation of pruriceptive spino-thalamic tract (STT) nociceptive neurons that convey pruritic information to the brain (Bautista et al., 2014; LaMotte et al., 2014). The generation and conductance of electrical signal in sensory pathways play an important role in the formation and maintenance of itch. A recent study suggested that the activity of MrgprA3$^+$ neurons was enhanced in a delayed contact hypersensitivity (CHS) model, a model of inflammatory itch and pain (Qu et al., 2014). But the electrophysiological property of MrgprA3$^+$ itch neurons in normal physiological condition remains unclear. The main reason is a lack of specific markers for MrgprA3$^+$ neurons.

Accordingly, we generated a strain of mice to label MrgprA3$^+$ neurons by a genetic approach. By expressing the tdTomato protein, these labeled neurons showed red fluorescence under fluorescent microscopy (Han et al., 2013). We observed the distribution of MrgprA3$^+$ neurons in DRG. Then we studied their action potential (AP) firing patterns to a train of depolarizing current injection by a patch-clamp technique. We also analyzed the parameters of the AP. Finally, we compared the difference of the voltage-gated potassium (Kv) current between positive and two subsets of negative MrgprA3 neurons (MrgprA3$^-$-non-Dil and MrgprA3$^-$-Dil neurons) and found that MrgprA3$^+$ neurons showed greater sustained Kv current than both two MrgprA3$^-$ neurons group. We expect that it can help us explain why there is the difference in the AP firing pattern between MrgprA3$^+$ and MrgprA3$^-$ neurons.

## 2. Results

### 2.1. MrgprA3$^+$ and MrgprA3$^-$ neurons connected to the skin are labeled by molecular genetic and retrograde tracing methods respectively

To specifically label MrgprA3$^+$ neurons in the DRG, we crossed *Mrgpra3$^{GFP-Cre}$* mice with Cre-dependent *ROSA26$^{tdTomato}$* reporter mice, and obtained *Mrgpra3$^{GFP-Cre}$; ROSA26$^{tdTomato}$* mice, as previously described (Han et al., 2013). The DRG sections from the homozygous *Mrgpra3$^{GFP-Cre}$; ROSA26$^{tdTomato}$* transgenic adult mice were used for the fluorescence imaging. The results clearly showed that the MrgprA3$^+$ neurons were marked by the coexpression of GFP and tdTomato protein (Fig. 1A–C). The green and red fluorescence could be displayed because the GFP was restricted to express in the cell nucleus with Cre recombinase and the tdTomato was in the cytoplasm (Han et al., 2013). We observed the distribution of DRG neurons on the L4–L6 levels sections and counted the percentage of MrgprA3$^+$ neurons on DRG sections under different fluorescent labeling. We found that about 97% of the GFP$^+$ neurons and tdTomato$^+$ neurons (283/292 from 2 mice) were co-expressed in a subset of small-diameter DRG neurons. This was consistent with the previous imaging results showing that the expression of GFP–Cre was tightly controlled by the endogenous Mrgpra3 promoter and that the tdTomato was restricted to be expressed in the MrgprA3$^+$ neurons (Han et al., 2013). This observation indicates that we are able to successfully breed the *Mrgpra3$^{GFP-Cre}$* and *ROSA26$^{tdTomato}$* transgenic mouse lines. The MrgprA3$^+$ neurons specifically labeled by the expression of GFP and tdTomato allow us to characterize the property of subtype neurons in DRG.

After the MrgprA3$^+$ neurons were identified, the MrgprA3$^-$ neurons specifically innervating the skin were also labeled by subcutaneous injection of Dil to the dorsal skin in *Mrgpra3$^{GFP-Cre}$* mice. In cultured DRG neurons (Fig. 2A–C) and DRG sections (Fig. 2D–F) from these labeled transgenic mice, MrgprA3$^+$ neurons were able to display both green (GFP) and red (Dil) fluorescence; by contrast, only red (Dil) but not green (GFP) labeled neurons were MrgprA3$^-$ neurons innervating the skin (MrgprA3$^-$-Dil). Additionally, neither tdTomato nor GFP neurons, we classified them as MrgprA3$^-$-non-Dil neurons.
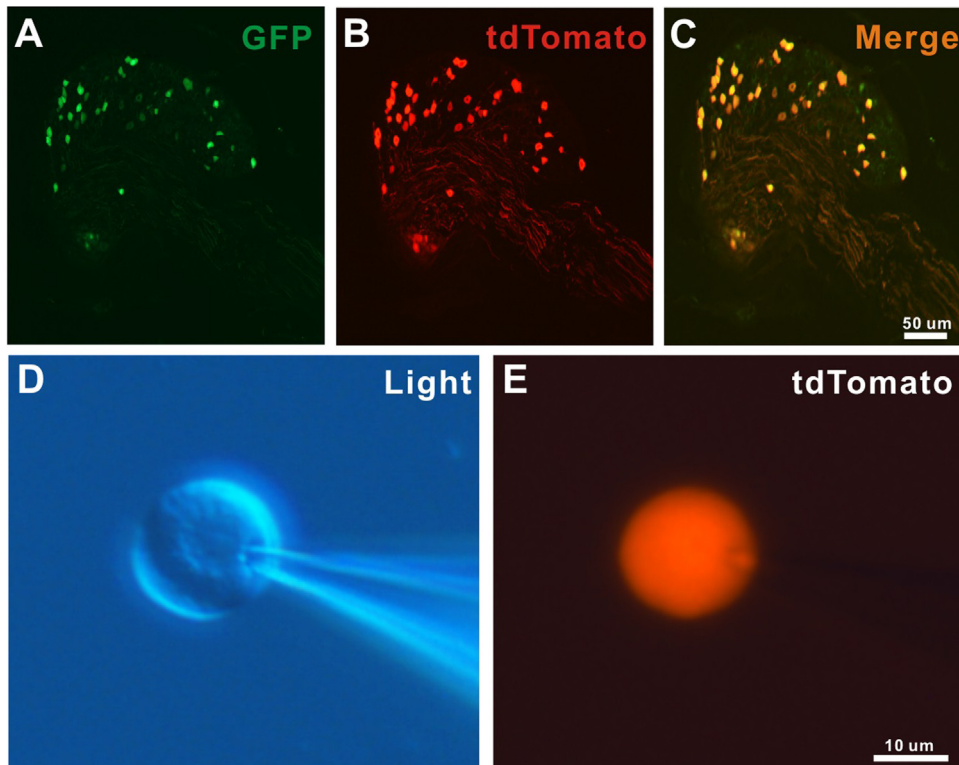
Fig. 1 – MrgprA3$^+$ neurons were identified by the expression of GFP and tdTomato. (A–C) The fluorescence imaging of DRG sections from adult homozygous MrgprA3$^{GFP-Cre}$; ROSA26$^{tdTomato}$ mice, the MrgprA3$^+$ neurons were marked by GFP (A) and tdTomato protein (B) and over 96% of GFP-expressing neurons coexpress with tdTomato (C). (D, E) MrgprA3$^+$ neurons for electrophysiological recording were shown in the bright field (D) and under fluorescent condition (E).
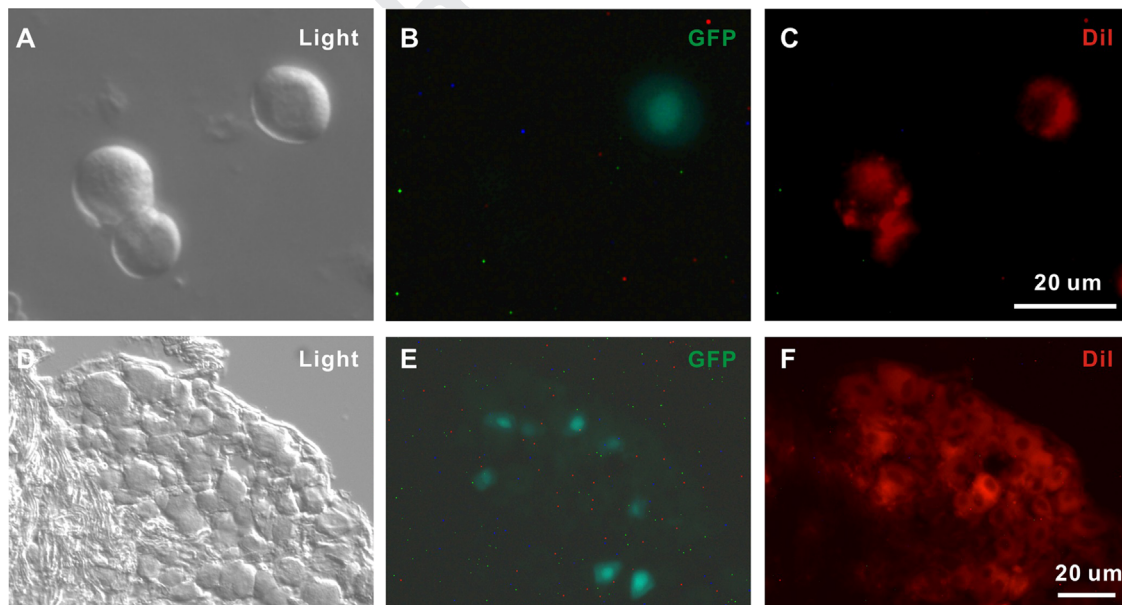


Fig. 2 – Cutaneous MrgprA3$^-$ neurons were labeled by DiI retrograde tracing in transgenic Mrgpra3$^{GFP-Cre}$ mice. (A–C) In cultured DRG neurons, representative images of MrgprA3$^+$ and MrgprA3$^-$-DiI neurons in bright field and under fluorescent condition. (D–F) In DRG cut section, representative image of MrgprA3$^+$ and MrgprA3$^-$-DiI neurons in bright field and fluorescent condition. Note that a subset of MrgprA3$^-$-DiI neuron was only marked by DiI.
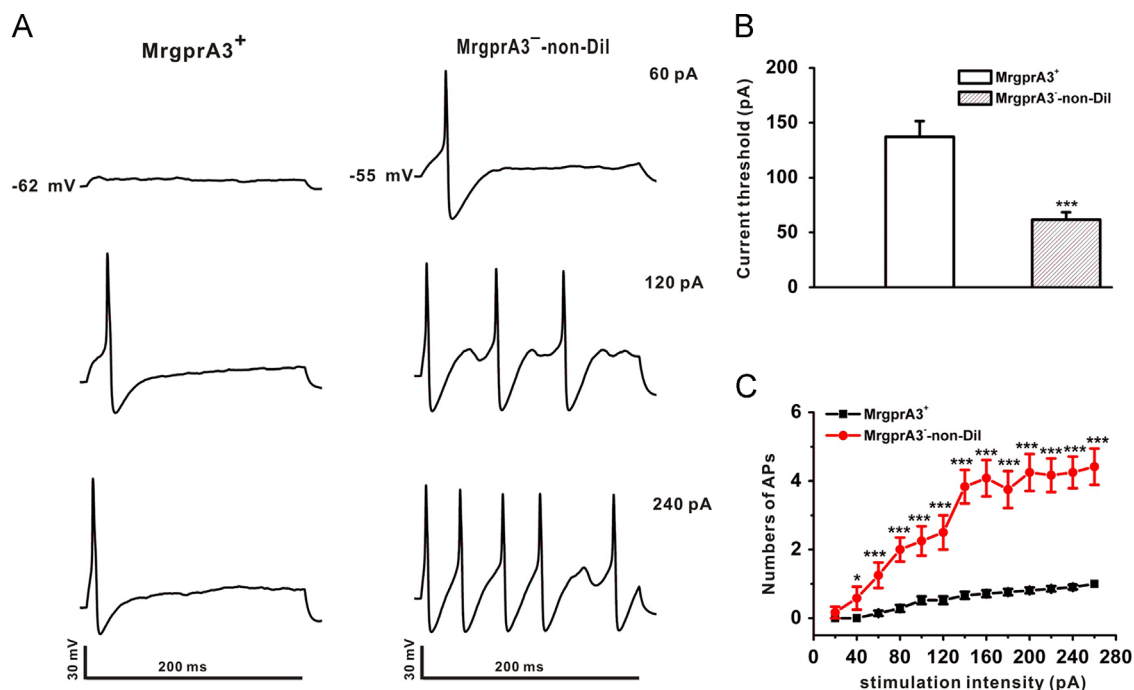
Fig. 3 – Depolarizing current evoked fewer APs in MrgprA3$^+$ neurons than in MrgprA3$^-$-non-Dil neurons. (A) Representative trace of AP firing induced by increasing intensities of depolarizing currents (pulse duration: 200 ms). (B) The mean current threshold to evoke AP in MrgprA3$^+$ neurons ($n=23$) was significantly higher than that in MrgprA3$^-$-non-Dil neurons ($n=21$). (C) The mean numbers of evoked APs in MrgprA3$^+$ neurons were significantly less than in MrgprA3$^-$-non-Dil neurons. Data are expressed as mean$\pm$SEM, $^*P<0.05$; $^{***}P<0.001$; as compared with MrgprA3$^+$ group, unpaired $t$-test.

## 2.2. MrgprA3$^+$ neurons fire less action potential to depolarizing current injection

MrgprA3$^+$ neurons with strong tdToamto fluorescence can be easily distinguished from MrgprA3$^-$-non-Dil neurons under a fluorescent microscope in the patch-clamp recording condition (Figs. 1D–E and 2C). To investigate the AP firing activity in the MrgprA3$^+$ and in the MrgprA3$^-$ neurons, we injected a train of depolarizing steps current ($\Delta=20$ pA) from 0 to 260 pA with a duration of 200 ms through electrodes to evoke AP firing in the whole cell current-clamp mode. The interval of each trace was 1000 ms. Following the increase of the stimulus current, MrgprA3$^-$-non-Dil neurons generated multiple spikes firing; however, MrgprA3$^+$ neurons only generated an AP, but there was a non-multiple spikes firing pattern in most cases (Fig. 3A). The mean current threshold required to induce MrgprA3$^+$ neurons ($n=23$) to generate the first AP was $137.1\pm14.4$ pA, but for MrgprA3$^-$-non-Dil neurons, the mean current threshold was $61.7\pm6.7$ pA ($n=21$, $P<0.001$, unpaired $t$-test) (Fig. 3B). In such a stimulating range of 40–260 pA current injection, the mean firing number of APs of MrgprA3$^-$-non-Dil neurons was more than the MrgprA3$^+$ neurons ($P<0.05$ or 0.001, unpaired $t$-test) (Fig. 3C). In MrgprA3$^-$ neurons that connect the skin (MrgprA3$^-$-Dil, $n=22$), repetitive firing pattern was also found in most case (Fig. 4A). In relative to MrgprA3$^+$ neurons, the current threshold was significantly smaller (Fig. 4B), and firing AP numbers were obviously increased (Fig. 4C).

## 2.3. MrgprA3$^+$ and MrgprA3$^-$ neurons show different characteristics of action potential

To determine why there is an AP firing difference between MrgprA3$^+$ and two subsets of MrgprA3$^-$ neurons, a series of depolarization injection currents with short 2 ms duration were used to induce a single intact AP shape (Fig. 5A). We measured the AP-related parameters from all recordings and compared their values between the MrgprA3$^+$ and two subsets of MrgprA3$^-$ neurons. As shown in Table 1, the overshoot, maximum rise slope and rise slope (10–90%) of MrgprA3$^+$ neurons were significantly larger than the MrgprA3$^-$-non-Dil ($P<0.05$ or 0.001, unpaired $t$-test). This indicated that the depolarizing speed of MrgprA3$^+$ neurons was significantly faster than MrgprA3$^-$-non-Dil neurons when an AP was generating. However, no significant difference was observed in upstroke phase between MrgprA3$^+$ and MrgprA3$^-$-Dil neurons. Moreover, the duration to 50% and 80% decay of MrgprA3$^+$ neurons was significantly longer than MrgprA3$^-$-non-Dil and MrgprA3$^-$-Dil neurons ($P<0.05$ or 0.01, unpaired $t$-test), suggesting that the after-depolarization speed of MrgprA3$^+$ neurons was slower than in the MrgprA3$^-$ neurons. Meanwhile, the diameter, cell capacitance, duration at 0 mV, half-width, threshold and input resistance were not significantly different between the MrgprA3$^+$ and two MrgprA3$^-$ neurons groups (Fig. 5B–G). However, the resting membrane potential (RMP) of MrgprA3$^+$ neurons ($-63.5\pm2.1$ mV) were significantly lower than in the MrgprA3$^-$-non-Dil and MrgprA3$^-$-Dil neurons ($-55.1\pm1.3$ mV, $-53.8\pm1.4$ mV, respectively; $P<0.001$, unpaired $t$-test) (Fig. 5H). Taken together, MrgprA3$^+$ neurons showed different AP-related
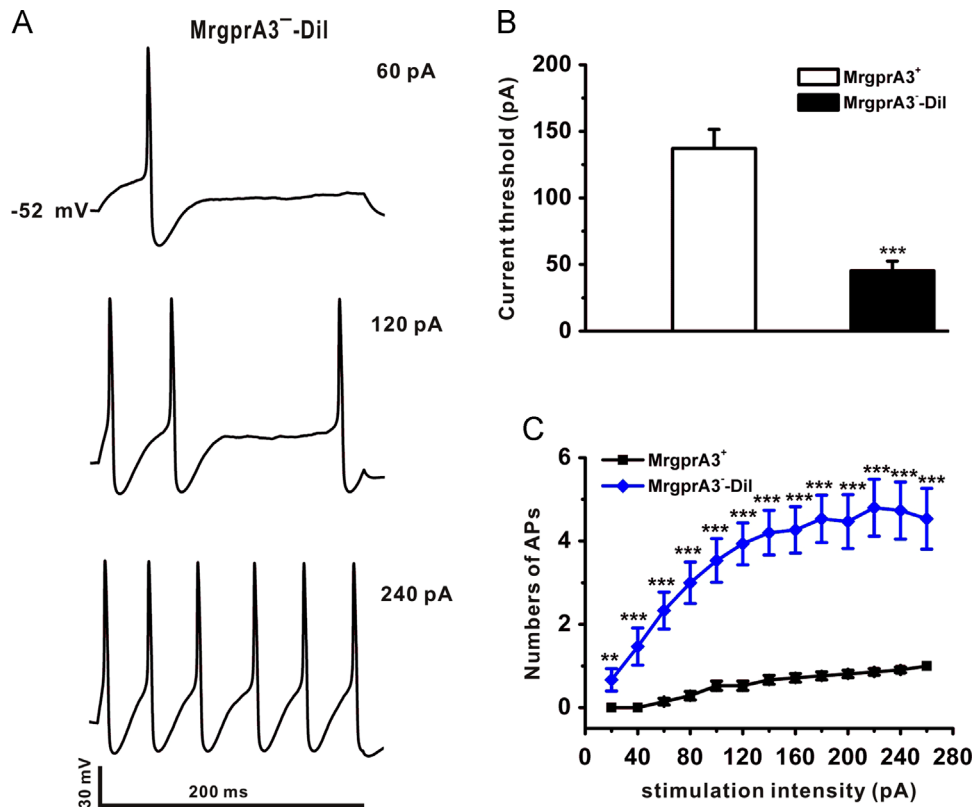
Fig. 4 – The firing activity of MrgprA3⁻-Dil neurons evoked by depolarizing current. (A) Representative trace of AP firing in MrgprA3⁻-Dil neurons induced by increasing depolarizing currents. (B) The mean current threshold to evoke AP in MrgprA3$^+$ neurons ($n=23$) was significantly higher than that in MrgprA3⁻-Dil neurons ($n=22$). (C) The mean numbers of evoked APs in MrgprA3$^+$ neurons were significantly less than in MrgprA3⁻-Dil neurons. Data are expressed as mean±SEM, **$P<0.01$; ***$P<0.001$; as compared with MrgprA3$^+$ group, unpaired $t$-test.
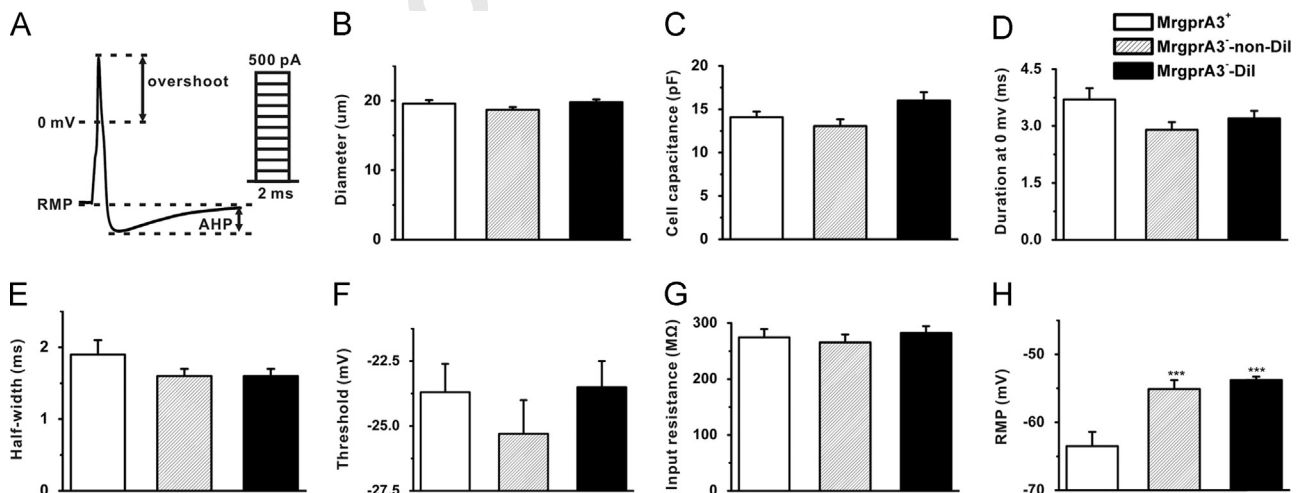


Fig. 5 – Extended electrophysiological parameters among MrgprA3$^+$ ($n=27$), MrgprA3⁻-non-Dil ($n=22$) and MrgprA3⁻-Dil neurons ($n=24$). (A) Representative AP shape evoked by depolarizing current ($\Delta=50$ pA, 2 ms) in a MrgprA3$^+$ neuron. (B) Diameter, (C) Cell capacitance, (D) Duration at 0 mV, (E) Half-width, (F) Threshold, (G) Input resistance, (H) RMP, resting membrane potential. Values are mean±SEM, ***$P<0.001$; as compared with MrgprA3$^+$ group, unpaired $t$-test.

**Table 1 – Electrophysiological parameters of MrgprA3⁺ and two subsets of MrgprA3⁻ neurons in whole-cell patch-clamp recording experiment.**

| | MrgprA3⁺ ($n=27$) | MrgprA3⁻-non-Dil ($n=22$) | MrgprA3⁻-Dil ($n=24$) |
|---|---|---|---|
| **Upstroke** | | | |
| Overshoot (mV) | 47.6±2.0 | 34.6±2.5[***] | 48.7 ± 1.8 |
| Time of overshoot (ms) | 58.7±0.4 | 59.5±0.5 | 60.0±1.2 |
| Maximum rise slope (mV/ms) | 79.2±6.7 | 51.4±7.1[*] | 80.0±8.1 |
| Time of maximum rise slope (ms) | 58.0±0.4 | 58.8±0.5 | 59.5±1.2 |
| Rise slope (10–90%) (mV/ms) | 68.1±5.6 | 45.8±6.1[*] | 74.6±7.4 |
| Rise time (10–90%) (ms) | 0.6±0.1 | 0.7±0.1 | 0.5±0.1 |
| **Downstroke** | | | |
| Max decay slope (mV/ms) | −27.4±1.5 | −28.8±2.5 | −30.3±2.2 |
| Time of max decay slope (ms) | 59.9±0.7 | 60.6±0.6 | 60.8±1.2 |
| Decay slope (90–10%) (mV/ms) | −22.8±1.5 | −23.9±2.1 | −25.3±1.7 |
| Decay time (90–10%) (ms) | 1.9±0.2 | 1.2±0.1 | 1.4±0.1 |
| **Afterpotential** | | | |
| AHP depth (mV) | 24.1±1.1 | 24.8±2.0 | 24.3±1.2 |
| Duration to 50% decay (ms) | 40.2±2.9 | 26.2±2.5[**] | 32.5±2.9[*] |
| Duration to 80% decay (ms) | 90.8±7.4 | 56.9±7.3[**] | 72.3±7.6[*] |

Data are presented by mean±SEM. [*]P<0.05; [**]P<0.01; [***]P<0.001; as compared with the MrgprA3⁺ group, unpaired t-test. AHP, after hyperpolarization; MrgprA3⁻-non-Dil, MrgprA3 negative neurons without labeled by Dil; MrgprA3⁻-Dil, MrgprA3 negative neurons labeled by Dil, which specifically innervate skin.
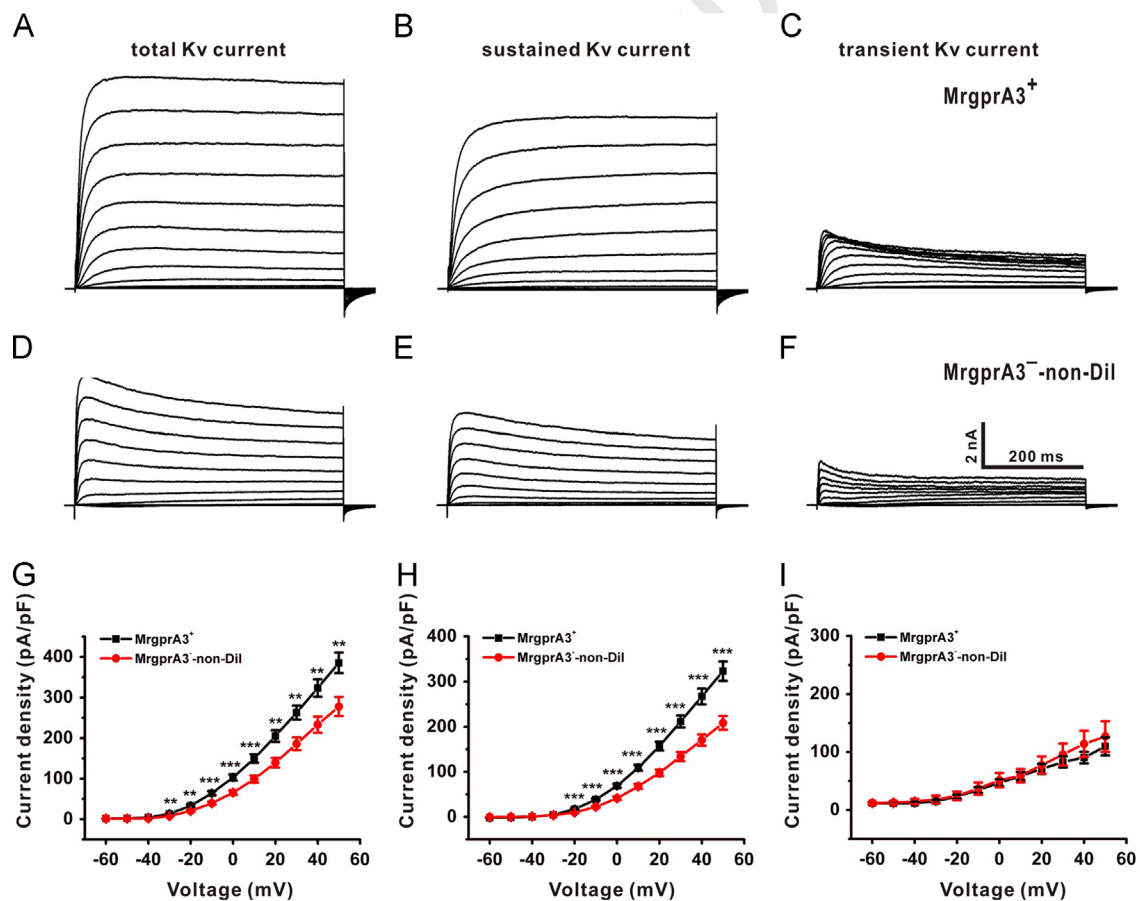


Fig.6 – MrgprA3⁺ neurons showed greater Kv currents than MrgprA3⁻-non-Dil neurons. (A–F) Representative traces of the total Kv current (A, D), sustained (B, E) and transient Kv currents (C, F) in MrgprA3⁺ and MrgprA3⁻-non-Dil neurons. (G) The mean density of total Kv currents of MrgprA3⁺ neurons ($n=22$) was significantly higher than that of MrgprA3⁻-non-Dil neurons ($n=20$). (H) The mean density of sustained Kv current was significantly higher in MrgprA3⁺ neurons than in MrgprA3⁻-non-Dil neurons. (H) There was no significant difference in the transient Kv currents between MrgprA3⁺ and MrgprA3⁻-non-Dil neurons. Data are expressed as mean±SEM, [*]P<0.05; [**]P<0.01; [***]P<0.001; as compared with MrgprA3⁻-non-Dil group, unpaired t-test.

parameters from two subsets of MrgprA3$^-$ neurons, suggesting that they have distinct membrane properties in the electrophysiology.

### 2.4. MrgprA3$^+$ neurons show greater voltage-gated potassium current than MrgprA3$^-$ neurons

MrgprA3$^+$ neurons exhibited significantly fewer AP firing numbers and lower RMP compared with two subsets of MrgprA3$^-$ neurons. Therefore, we further tested whether there was variation in the voltage-gated K$^+$ (Kv) currents, since Kv channels play an important role in the regulation of neuronal firing frequency and in the formation of RMP (Maljevic and Lerche, 2013). In general, the total Kv current consisted of sustained Kv current and transient Kv current (A-type Kv current) (Fan et al., 2011). In the whole cell voltage-clamp recording configuration, the total Kv current was evoked by a train of test pulses from $-60$ mV to $+50$ mV with 500 ms durations, preceded by a 1000 ms prepulse to $-100$ mV (Fig. 6A and D). The $-40$ mV holding potential with 1000 ms duration was used to inactive the transient Kv currents (Fig. 6B and E). The subtraction of the current traces induced at two holding potentials yielded the transient Kv currents (Fig. 6C and F). The mean density of total Kv currents in the MrgprA3$^+$ neurons ($n=22$) was significantly greater compared to the MrgprA3$^-$-non-Dil ($n=20$) from $-30$ mV to $+50$ mV ($P<0.01$ or 0.001, unpaired $t$-test) (Fig. 6G). Our data also indicated that the mean density of sustained Kv currents in the MrgprA3$^+$ neurons ($n=22$) was nearly 1.6 times larger than in the MrgprA3$^-$-non-Dil ($n=20$, $P<0.001$, unpaired $t$-test) (Fig. 6H). But for the transient Kv currents (Fig. 6I), there was no difference between the MrgprA3$^+$ ($n=22$) and

MrgprA3$^-$-non-Dil ($n=20$). For MrgprA3$^-$-Dil neurons ($n=22$), there were also significantly greater total ($P<0.05$, 0.01 or 0.001, unpaired $t$-test) (Fig. 7A and D) and sustained (Fig. 7B and E) Kv current density compared with MrgprA3$^+$ neurons. Similar with MrgprA3$^-$-non-Dil neurons, the transient Kv current (Fig. 7C and F) showed no significant difference between MrgprA3$^+$ and MrgprA3$^-$-Dil neurons.

The significantly greater sustained Kv current in MrgprA3$^+$ neurons seems to reduce its AP firing activity. We pharmacologically blocked sustained Kv channels with 25 mM TEA (Cao et al., 2010; Vydyanathan et al., 2005) and then measured AP firing activity using protocol identical with Figs. 3 and 4. The MrgprA3$^+$ neurons ($n=10$) fired multiple APs after TEA perfusion in the bath solution for 3 min. When the TEA was washed out, the same stimulus current induced lesser AP (Fig. 8A). The statistic data also indicated that the mean AP number induced in the various current injection was significantly greater after TEA blocking compared with control and wash condition (Fig. 8B). Meanwhile, the neurons in TEA condition showed significantly lower current threshold (Fig. 8C). However, no significant differences existed between control and wash condition. Taken together, blocking sustained Kv channel with TEA increases MrgprA3$^+$ neurons' AP firing activity.

## 3. Discussion

MrgprA3 receptors are restricted to express in subsets of small-diameter sensory neurons in DRG and trigeminal ganglia neurons and contributed to CQ-induced itch (Liu et al., 2009). Our previous study found that MrgprA3$^+$ neurons are
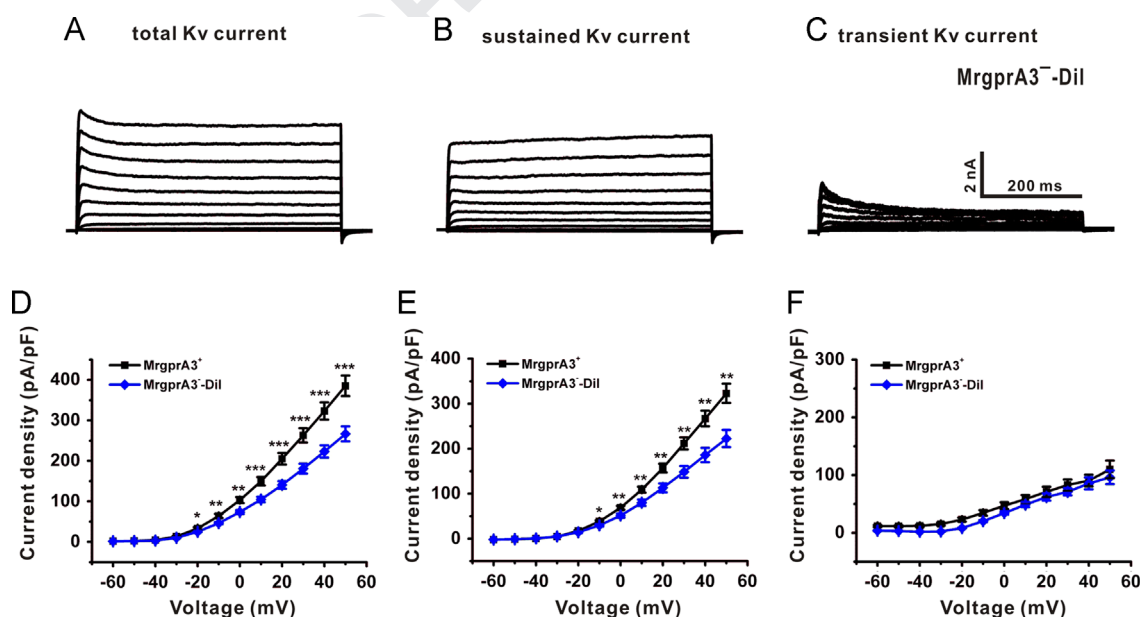


Fig. 7 – MrgprA3$^+$ neurons showed greater Kv currents than MrgprA3$^-$-Dil neurons. (A–F) Representative traces of the total (A), sustained (B) and transient Kv currents (C) in MrgprA3$^-$-Dil neurons. (D) The mean density of total Kv currents of MrgprA3$^+$ neurons ($n=22$) was significantly higher than that of MrgprA3$^-$-Dil neurons ($n=22$). (H) The mean density of sustained Kv current was significantly higher in MrgprA3$^+$ neurons than in MrgprA3$^-$-Dil neurons. (H) No significant difference was existed in the transient Kv currents between MrgprA3$^+$ and MrgprA3$^-$-Dil neurons. Data are expressed as mean±SEM, $^*P<0.05$; $^{**}P<0.01$; $^{***}P<0.001$; as compared with MrgprA3$^-$-Dil group, unpaired $t$-test.
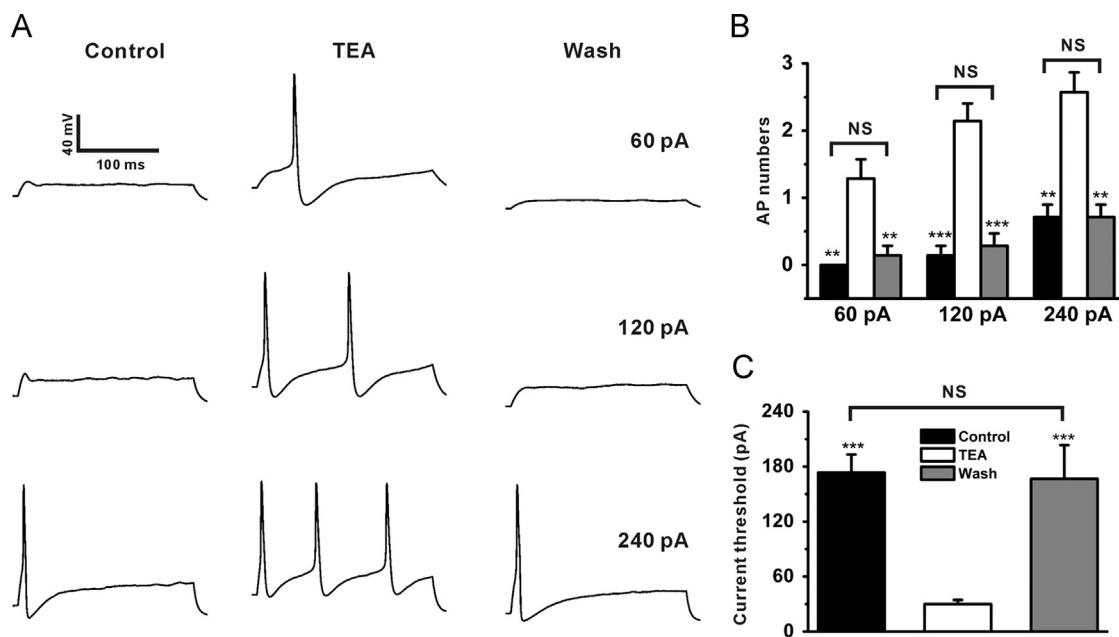
**Fig. 8 – Inhibition of sustained Kv channels enhanced MrgprA3$^+$ neurons' AP firing activity. (A) Representative trace showing that blocking sustained Kv channels with 25 mM TEA induced MrgprA3$^+$ neurons generating multiple AP firing activity. (B) Blocking TEA-sensitive sustained Kv channels increased AP numbers evoked in various stimulus current (in A). (C) The current threshold of MrgprA3$^+$ neurons ($n=10$) was significantly reduced in TEA condition. Values are mean$\pm$SEM, **$P<0.01$; ***$P<0.001$; NS, no significant difference; as compared with TEA group. Paired $t$-test was used to analysis.**

specifically linked to itch but not to pain sensation—regardless of the stimulus type used to activate the neurons (Han et al., 2013). TRPA1 plays an important role in the downstream target of MrgprA3 receptor and mediates CQ-induced histamine-independent itch behavior in mice (Wilson et al., 2011). Although advances of MrgprA3 are occurring in the itch research field, the electrophysiological property of MrgprA3 neurons still has not been reported. We employed molecular genetic means to specifically label MrgprA3 neurons by the expression of GFP and tdTomato. We could clearly observe these MrgprA3 neurons in DRG under fluorescence microscopy and study their electrophysiological properties by selecting them to record. In the present study, we first investigated the electrophysiological properties of itch-specific MrgprA3$^+$ neurons. Meanwhile, we also recorded the same size MrgprA3$^-$-non-Dil and cutaneous MrgprA3$^-$-Dil neurons as controls; the majority of them might be nociceptors (Basbaum et al., 2009).

Our results indicated that the itch-specific MrgprA3$^+$ neurons had significant differences in AP firing pattern than MrgprA3$^-$-non-Dil and MrgprA3$^-$-Dil neurons. Both MrgprA3$^-$-non-Dil and MrgprA3$^-$-Dil neurons could generate multiple APs firing although the number and pattern of APs firing were diverse for each neuron, but MrgprA3$^+$ neurons generated non-multiple APs firing in spite of following the increase of stimulus current in most instances. The APs firing pattern reflects the physiological properties of a neuron. Every kind of pattern—generally including spontaneous firing, regular firing, bursting firing, and tonic firing—indicates signal conductance of a single neuron (Tang and Wang, 2002). The APs firing activity in DRG neurons from normal physiological mice differs from mice with the pain or itch model

(Amir et al., 2002; Hachisuka et al., 2010; Schafers et al., 2003). In the contact hypersensitivity (CHS) model, MrgprA3$^+$ neurons became hyper-excitable and generated multiple spikes in response to depolarizing current (Qu et al., 2014). MrgprA3 itch neurons showed favorable to generating single AP in most instances, this firing feature may be an inherent characteristic of itch neurons.

It seems that a non-multiple firing pattern is the property of the MrgprA3$^+$ neurons only in normal physiological mice. The factors affecting the AP firing activity are numerous; many of the factors belong to ion channels (Waxman and Zamponi, 2014). For example, the reduction of M current's density in small-sized DRG neurons contributes to the atopic APs firing in bone cancer pain in rats (Zheng et al., 2013). The deceased A-type Kv current increased the AP's firing frequency of the IB4$^+$ DRG neurons (Vydyanathan et al., 2005). We studied the diversity in APs firing pattern between the MrgprA3$^+$ and two subsets of MrgprA3$^-$ neurons by analyzing the AP-related parameters, which were recorded by a short 2 ms depolarizing current injection to ensure the intact shape of the AP. The AP is the basic unit of excitability and physiological function for sensory neurons. The nociceptive or pruriceptive substances from endogenous or exogenous environment activate the nerve endings and generate APs that are conducted by their axons to the spinal cord. Finally, after processing of this nociceptive or pruriceptive information, a sensation of pain or itch is formed in the brain (Akiyama et al., 2014; Bautista et al., 2014). Generally, an intact AP shape consists of a depolarization, repolarization, hyperpolarization, and afterdepolarization phase (Waddell and Lawson, 1990). Different ion channels contribute to the each phase of the AP. The voltage-gated Na$^+$ (Nav) channels

are mainly involved in the depolarization phase (Blair and Bean, 2002), and the Kv channels are mainly involved in the repolarization and hyperpolarization phase (Liu and Bean, 2014; Mitterdorfer and Bean, 2002).

Our study indicated that significant differences exist in the depolarization phase between the MrgprA3$^+$ and general MrgprA3$^-$-non-Dil neurons, but no significant difference for cutaneous sensory MrgprA3$^-$-Dil neurons. Besides, the duration to 50% decay and duration to 80% decay were also significantly greater in the MrgprA3$^+$ neurons compared with two MrgprA3$^-$ neurons group. This suggests that the time interval to evoke the next AP in MrgprA3$^+$ neurons is longer than in MrgprA3$^-$ neurons, which might be the important reason for non-multiple spikes in MrgprA3$^+$ neurons. Meanwhile, the lower resting membrane potential of MrgprA3$^+$ neurons indicates their higher current threshold to evoke AP compared with MrgprA3$^-$ neurons.

The Kv channels play an important role in determining the neuronal firing frequency (Maljevic and Lerche, 2013). In general, distinct Kv channels are widely expressed in sensory neurons and Kv currents can be divided mainly into sustained Kv and transient Kv currents (Rasband et al., 2001; Tsantoulas et al., 2012). It is important that sustained Kv and transient Kv currents were involved in regulating action potential and the rest membrane potential (Ritter et al., 2015; Takeda et al., 2011). In this study, we found that both the mean current density of the total and the sustained Kv current were greater in MrgprA3$^+$ neurons than in MrgprA3$^-$-non-Dil and MrgprA3$^-$-Dil neurons. This might be a reason that there is the more negative RMP in MrgprA3$^+$ neurons than in MrgprA3$^-$ neurons. This kind of phenomenon has also been reported in other studies (Ritter et al., 2015; Takeda et al., 2011). Importantly, pharmacological blocking sustained Kv channels significantly increased the MrgprA3$^+$ neurons AP firing activity, indicating that the greater sustained Kv current decreases MrgprA3$^+$ neurons' excitability.

In summary, our results demonstrated that MrgprA3$^+$ neurons have lower excitability than the same size MrgprA3$^-$-non-Dil and MrgprA3$^-$-Dil neurons. MrgprA3$^+$ neurons exhibit decreased AP firing activity; this may result from its high density of sustained Kv current. The fewer spikes in MrgprA3$^+$ neurons help us to further understand the physiological functions of itch-specific neurons, and may provide the strategy and method for itch disease therapy.

# 4. Experimental procedures

## 4.1. Animals

The mice were C57BL/6 males or female, 6–8 weeks of age, weighing 24–32 g. For *Mrgpra3$^{GFP-Cre}$* mice, our previous study indicated that GFP–Cre fusion protein was expressed under the control of the *Mrgpra3* promoter. We crossed *Mrgpra3$^{GFP-Cre}$* mice with Cre-dependent *ROSA26$^{tdTomato}$* reporter mice; Cre-active neurons were marked by the expression of tdTomato (Han et al., 2013). The genotype of the offspring was determined by PCR analysis. Because of the strong fluorescence of the tdTomato protein, MrgprA3$^+$ neurons could be visualized directly and distinguished easily for electrophysiological recording by fluorescence microscopy. The mice were housed with a 12 h light-dark cycle at 22 °C, with free access to water and food. All experiments were conducted in accordance with the National Science Foundation of China Guidelines for the Care and Use of Laboratory Animals.

## 4.2. Retrograde tracing of cutaneous MrgprA3 negative neurons

The transgenic *Mrgpra3$^{GFP-Cre}$* mice were used to retrograde tracing of MrgprA3 negative neurons that connect skin. The mice were anaesthetized with 1% sodium pentobarbital and the hair in dorsal skin was removed by using animal hair clipper. To diminish lesion to the skin, an insulin syringe was used to inject 1,1′-Dioctadecyl-3,3,3′,3′-tetramethylindocarbocyanine perchlorate (Dil, 0.25% in DMSO, Sigma). 50 μl Dil was subcutaneously injected to the different site of dorsal skin, about 5 μl Dil for each injection site. After 10 days later, the operated mice were used for cell culture and DRG section imaging.

## 4.3. Fluorescence imaging of the DRG section

The 8-week-old homozygous *Mrgpra3$^{GFP-Cre}$*; *ROSA26$^{tdTomato}$* transgenic mice and 6 week-old retrograde transgenic *Mrgpra3$^{GFP-Cre}$* mice were deeply anaesthetized with 1% sodium pentobarbital. Perfusion with 25 ml cold 0.01 M phosphate buffer solution (PBS) was followed by 30 ml cold 4% paraformaldehyde (PFA) in 0.01 M PBS, PH7.4. The DRG in L4–L6 spinal level was collected and post-fixed into 4% PFA at 4 °C for 2 h then soaked in 30% sucrose solution in 0.01 M PBS for 24 h. The DRG tissues were embedded with OCT and rapidly frozen at $-20$ °C. The frozen DRG sections were cut into 10 μm thickness using a cryostat (Leica, GM1950, Germany). All sections were collected in slides and washed three times for each 5 min with 0.01 M PBS. The prepared DRG sections were viewed and captured using an Olympus fluorescence microscope (Olympus, BX51, Japan). Finally, the images were acquired and overlapped by Stereo Investigator software (Stereo Investigator 10, MBF, USA). For the DRG section of retrograde tracing *Mrgpra3$^{GFP-Cre}$* mice, the imaging was viewed and captured using fluorescence microscopy (ZEISS, Axio Oberver D1, Germany).

## 4.4. Cell culture

The 3-4-week-old homozygous *Mrgpra3$^{GFP-Cre}$*; *ROSA26$^{tdTomato}$* transgenic mice and the retrograded *Mrgpra3$^{GFP-Cre}$* mice were used for cell culture. DRG from all spinal levels of mice were collected in cold DH10 medium (90% DMEM/F-12, 10% FBS, 100 U/ml penicillin, 100 ug/ml streptomycin, Gibco) and treated with enzyme solution (1 mg/ml Collagenase Type I and 5 mg/ml Dispase in HPBS without Ca$^{2+}$ and Mg$^{2+}$, Invitrogen) at 37 °C for 25 min. The DRG tissue was scattered with a fire-polished Pasteur pipette. After centrifugation, cells were re-suspended in warm (37 °C) DH10 with NGF (20 ng/ml), plated on glass coverslips coated with poly-D-lysine (0.5 mg/ml) and laminine (10 μg/ml). They were cultured in an incubator (95% O$_2$ and 5% CO$_2$) at 37 °C. These neurons were used for electrophysiological recordings within 24 h.

## 4.5. Electrophysiological recording

MrgprA3$^+$ and MrgprA3$^-$-non-Dil neurons were identified by the red fluorescence of tdTomato protein using fluorescence microscopy (ZEISS, Axio Oberver D1, Germany). MrgprA3$^-$-Dil neurons were labeled by Dil but without GFP. Cover-slips were transferred into a chamber with the extracellular solution. Whole-cell current clamp and voltage-clamp recording experiments were performed at room temperature (23–25 °C) using a Multi-clamp 700B amplifier and Digital 1440 with pClamp10 software (Molecular Devices, USA).

Signals were sampled at 20 kHz and filtered at 2 kHz. The patch pipettes were pulled from borosilicate glass capillaries using a P-97 micropipette puller (Sutter Instrument) and had a resistance of 3–4 MΩ for patch-clamp recordings. The series resistance was routinely compensated at 60–80%. The resting membrane potential (RMP) was recorded for each neuron under the current-clamp mode after stabilization (within 3 min). Neurons whose seal resistance was below 1 GΩ after breaking the cell membrane and whole-cell recording formation were excluded from analysis. The liquid junction potential was 8 mV and corrected. A single intact action potential was induced by a series of depolarizing current steps, each of 2 ms duration, increments of 50 pA through the recording electrode. For the APs firing-evoked test, each neuron was injected in a series of depolarizing current steps, 200 ms duration, increments of 20 pA. The current threshold was defined as the minimum injection current required eliciting an AP. The input resistance was measured from the slope of a steady-state current–voltage plot in response to a series of hyperpolarizing current steps from −200 to −50 pA (Qu et al., 2014). The other AP-related parameters were measured in Clampfit software. The internal solution contained the following (in mM): KCl 135, MgATP 3, Na$_2$ATP 0.5, CaCl$_2$ 1.1, EGTA 2, Glucose 5, with pH adjusted to 7.38 using KOH, and osmolarity adjusted to 300 mOsm with sucrose. The external solution contained the following (in mM): NaCl 140, KCl 4, CaCl$_2$ 2, MgCl$_2$ 2, HEPES 10, Glucose 5, with pH adjusted to 7.4 using NaOH, and osmolarity adjusted to 310 mOsm with sucrose (Liu et al., 2009). The TEA (purchased from Sigma, USA) was dissolved in distilled water as stock solution and kept frozen in aliquots. The stock TEA solution was diluted to 25 mM concentration with bath solution before use. Two independent syringes were used to perfuse TEA solution and bath solution respectively, the solutions was delivered to the recording chamber by gravity.

For Kv current recording, the intracellular pipette solution contained the following (in mM): potassium gluconate 120, KCl 20, MgCl$_2$ 2, EGTA 10, HEPES 10, and MgATP 4 (pH 7.3 with KOH, 310 mOsm). We minimized the Na$^+$ and Ca$^{2+}$ component in voltage-gated potassium current recording by using an extracellular solution composed of the following (in mM): choline chloride 150, KCl 5, CdCl$_2$ 1, CaCl$_2$ 2, MgCl$_2$ 1, HEPES 10, and glucose 10 (pH 7.4 with Tris base, 320 mOsm) (Zhao et al., 2013). The total Kv current was evoked by a series of 500 ms test pulses ranging from −60 to +50 mV in 10 mV steps, preceded by a 1000 ms holding potential in −100 mV. The command potential protocol was repeated from a holding potential of −40 mV to isolate sustained Kv current. Total Kv current subtracts sustained Kv current to yield transient Kv current (Fan et al., 2011). For the current traces, the current density was obtained by dividing the mean current by the cell capacitance, but for the transient Kv current, the peak current was normalized. All the chemical reagents used in electrophysiological recording were purchased from Sigma (USA).

## 4.6. Data analysis

Electrophysiological data were analyzed and fitted using Clampfit (Axon Instruments, Foster City, CA) and Origin Pro 8 (Origin Lab, USA) software. All the data were analyzed with unpaired Student's $t$-tests or Paired $t$-test and expressed as mean±standard errors of the means (S.E.M). The statistical significance was set at $P < 0.05$.

## Conflict of interest

The authors declare that they have no competing interests.

R E F E R E N C E S

Akiyama, T., et al., 2014. Behavioral model of itch, alloknesis, pain and allodynia in the lower hindlimb and correlative responses of lumbar dorsal horn neurons in the mouse. Neuroscience 266, 38–46.

Amir, R., Michaelis, M., Devor, M., 2002. Burst discharge in primary sensory neurons: triggered by subthreshold oscillations, maintained by depolarizing afterpotentials. J. Neurosci. 22, 1187–1198.

Basbaum, A.I., et al., 2009. Cellular and molecular mechanisms of pain. Cell 139, 267–284.

Bautista, D.M., Wilson, S.R., Hoon, M.A., 2014. Why we scratch an itch: the molecules, cells and circuits of itch. Nat. Neurosci. 17, 175–182.

Blair, N.T., Bean, B.P., 2002. Roles of tetrodotoxin (TTX)-sensitive Na$^+$ current, TTX-resistant Na$^+$ current, and Ca$^{2+}$ current in the action potentials of nociceptive sensory neurons. J. Neurosci. 22, 10277–10290.

Cao, X.H., et al., 2010. Reduction in voltage-gated K$^+$ channel activity in primary sensory neurons in painful diabetic neuropathy: role of brain-derived neurotrophic factor. J. Neurochem. 114, 1460–1475.

Dong, X., et al., 2001. A diverse family of GPCRs expressed in specific subsets of nociceptive sensory neurons. Cell 106, 619–632.

Fan, N., et al., 2011. Increased Na$^+$ and K$^+$ currents in small mouse dorsal root ganglion neurons after ganglion compression. J. Neurophysiol. 106, 211–218.

Hachisuka, J., et al., 2010. Responsiveness of C neurons in rat dorsal root ganglion to 5-hydroxytryptamine-induced pruritic stimuli in vivo. J. Neurophysiol. 104, 271–279.

Han, L., et al., 2013. A subpopulation of nociceptors specifically linked to itch. Nat. Neurosci. 16, 174–182.

Ikoma, A., et al., 2006. The neurobiology of itch. Nat. Rev. Neurosci. 7, 535–547.

Klein, A., Carstens, M.I., Carstens, E., 2011. Facial injections of pruritogens or algogens elicit distinct behavior responses in rats and excite overlapping populations of primary sensory and trigeminal subnucleus caudalis neurons. J. Neurophysiol. 106, 1078–1088.

LaMotte, R.H., Dong, X., Ringkamp, M., 2014. Sensory neurons and circuits mediating itch. Nat. Rev. Neurosci. 15, 19–31.

Liu, P.W., Bean, B.P., 2014. Kv2 channel regulation of action potential repolarization and firing patterns in superior cervical ganglion neurons and hippocampal CA1 pyramidal neurons. J. Neurosci. 34, 4991–5002.

Liu, Q., et al., 2009. Sensory neuron-specific GPCR Mrgprs are itch receptors mediating chloroquine-induced pruritus. Cell 139, 1353–1365.

Liu, Q., et al., 2012. Mechanisms of itch evoked by beta-alanine. J. Neurosci. 32, 14532–14537.

Liu, T., Ji, R.R., 2013. New insights into the mechanisms of itch: are pain and itch controlled by distinct mechanisms? Pflugers Arch. 465, 1671–1685.

Maljevic, S., Lerche, H., 2013. Potassium channels: a review of broadening therapeutic possibilities for neurological diseases. J. Neurol. 260, 2201–2211.

Mitterdorfer, J., Bean, B.P., 2002. Potassium currents during the action potential of hippocampal CA3 neurons. J. Neurosci. 22, 10106–10115.

Paus, R., et al., 2006. Frontiers in pruritus research: scratching the brain for more effective itch therapy. J. Clin. Investig. 116, 1174–1186.

Qu, L., et al., 2014. Enhanced excitability of MRGPRA3- and MRGPRD-positive nociceptors in a model of inflammatory itch and pain. Brain 137, 1039–1050.

Rasband, M.N., et al., 2001. Distinct potassium channels on pain-sensing neurons. Proc. Natl. Acad. Sci. USA 98, 13373–13378.

Ritter, D.M., et al., 2015. Dysregulation of kv3.4 channels in dorsal root Ganglia following spinal cord injury. J. Neurosci. 35, 1260–1273.

Schafers, M., et al., 2003. Increased sensitivity of injured and adjacent uninjured rat primary sensory neurons to exogenous tumor necrosis factor-alpha after spinal nerve ligation. J. Neurosci. 23, 3028–3038.

Schmelz, M., 2005. Itch and pain. Dermatol. Ther. 18, 304–307.

Sikand, P., Dong, X., LaMotte, R.H., 2011. BAM8-22 peptide produces itch and nociceptive sensations in humans independent of histamine release. J. Neurosci. 31, 7563–7567.

Takeda, M., et al., 2011. Potassium channels as a potential therapeutic target for trigeminal neuropathic and inflammatory pain. Mol. Pain 7, 5.

Tang, Z.X., Wang, S.R., 2002. Discharge patterns evoked by depolarizing current injection in basal optic nucleus neurons of the pigeon. Brain Res. Bull. 58, 371–376.

Tsantoulas, C., et al., 2012. Sensory neuron downregulation of the Kv9.1 potassium channel subunit mediates neuropathic pain following nerve injury. J. Neurosci. 32, 17502–17513.

Vydyanathan, A., et al., 2005. A-type voltage-gated K$^+$ currents influence firing properties of isolectin B4-positive but not isolectin B4-negative primary sensory neurons. J. Neurophysiol. 93, 3401–3409.

Waddell, P.J., Lawson, S.N., 1990. Electrophysiological properties of subpopulations of rat dorsal root ganglion neurons in vitro. Neuroscience 36, 811–822.

Waxman, S.G., Zamponi, G.W., 2014. Regulating excitability of peripheral afferents: emerging ion channel targets. Nat. Neurosci. 17, 153–163.

Wilson, S.R., et al., 2011. TRPA1 is required for histamine-independent, Mas-related G protein-coupled receptor-mediated itch. Nat. Neurosci. 14, 595–602.

Zhao, X., et al., 2013. A long noncoding RNA contributes to neuropathic pain by silencing Kcna2 in primary afferent neurons. Nat. Neurosci. 16, 1024–1031.

Zheng, Q., et al., 2013. Suppression of KCNQ/M (Kv7) potassium channels in dorsal root ganglion neurons contributes to the development of bone cancer pain in a rat model. Pain 154, 434–448.

Zylka, M.J., et al., 2003. Atypical expansion in mice of the sensory neuron-specific Mrg G protein-coupled receptor family. Proc. Natl. Acad. Sci. USA 100, 10043–10048.